OBSERVATOIRE DE PARIS – PSL

NATIONAL INSTITUTE OF ADVANCED INDUSTRIAL SCIENCE AND TECHNOLOGY (AIST)

TOHOKU UNIVERSITY

MASTER THESIS

4 MONTHS

STUDY OF UTPS-TB SIMULANTS VALIDITY AS PHOBOS SURFACE ANALOGUES

AUTHOR:

Emma VELLARD

SUPERVISORS:

Moe MATSUOKA (AIST)

Tomoki NAKAMURA (Tohoku University)

An internship report submitted in fulfilment of the requirements
for the degree of Master's in Space Science and Technology in the
M2 Planetary Science and Space Exploration Track

Words count: 11316

36 pages

Sendai, Japan

June 23rd, 2023

ABSTRACT

ENGLISH

The origin of the two Martian moons, Phobos and Deimos, is still a subject of controversy to this day and can be broken down into two main theories: the giant impact scenario and the asteroid capture scenario. The MMX[1] mission has been developed to gather data in the Martian system and collect samples from the surface of Phobos for study in laboratory. In preparation for these results, the UTPS[2] simulants were developed to study different mineralogical and physical properties according to the based theory. By analysing these simulants using spectroscopy in the visible to near-infrared range, it has been possible to identify the main phyllosilicates and carbonates present in the sample and to compare the reflectance spectra obtained with those collected on Phobos surface by CRISM[3] instrument onboard MRO[4] mission. Additionally the comparison suggests the reflectance difference cannot be fully explained by grain size difference but can be the result of space weathering and organic composition. The analysis has been realized in OROCHI[5] and MIRS[6] conditions, instruments onboard MMX mission which will be essential in identifying the 2.7-2.8µm phyllosilicates peak.

FRENCH

L'origine des deux lunes martiennes, Phobos et Deimos, est encore aujourd'hui un sujet de controverse et peut être divisée en deux théories principales : le scénario de l'impact géant et le scénario de la capture d'astéroïdes. La mission MMX a été développée pour recueillir des données dans le système martien et collecter des échantillons de la surface de Phobos pour les étudier en laboratoire. En préparation de ces résultats, les simulants UTPS ont été développés pour étudier différentes propriétés minéralogiques et physiques selon la théorie basée. En analysant ces simulants par spectroscopie dans le domaine du visible et du proche infrarouge, il a été possible d'identifier les principaux phyllosilicates et carbonates présents dans l'échantillon et de comparer les spectres de réflectance obtenus avec ceux collectés à la surface de Phobos par l'instrument CRISM à bord de la mission MRO. En outre, la comparaison suggère que la différence de réflectance ne peut pas être entièrement expliquée par la différence de taille des grains, mais peut être le résultat de l'altération de l'espace et de la composition organique. L'analyse a été réalisée dans les conditions OROCHI et MIRS, instruments embarqués sur la mission MMX qui seront essentiels pour identifier le pic de phyllosilicates de 2.7-2.8µm.

---

[1] Martian Moons eXploration.
[2] University of Tokyo Phobos Simulants.
[3] Compact Reconnaissance Imaging Spectrometer for Mars.
[4] Mars Reconnaissance Orbiter.
[5] Optical RadiOmeter composed of CHromatic Imagers.
[6] MMX InfraRed Spectrometer.

TABLE OF CONTENTS

FIGURES

TABLES

1. INTRODUCTION – THE MARTIAN SYSTEM

The Martian moons, Phobos and Deimos, have been studied by various space missions in recent years, providing information about their physical properties and mineralogical composition, but without providing an answer to the question of their origin. Two main theories are currently the most likely: the giant impact scenario and the asteroid capture scenario. Both hypotheses are controversial, and in an attempt to provide some answers, the space agencies NASA and JAXA have developed the MMX mission. In particular, it will make it possible to obtain spectra of the surface of the two moons and collect samples for further analysis on their return to Earth. To prepare for this mission, it is essential to anticipate likely outcomes. To this end, the UTPS simulants (University of Tokyo Phobos Simulants) have been developed. Based on the different scenarios, these simulants come in three versions defined according to their composition: TB (Tagish lake Based), IB (Impact theory Based), S (Simpler). For the asteroid capture scenario, the UTPS-TB simulants are based on a composition close to that of the most primitive bodies in the Solar System. In that case, asteroids as Ryugu are the best analogue to design such sample powder. The aim of creating these simulants is to get as close as possible to the spectra currently known for the surface of Phobos. Several factors could have an impact on their reflectance, in particular the size of the grains present on the surface, the porosity of the grains or their mineral composition. Studying the dependence of these points in these simulants could allow to confirm their validity to represent Phobos surface characteristics based on the spectra acquired to date with CRISM instrument of MRO spacecraft. In a few years, the MMX mission will verify the validity of both hypothesis with its mainly two of its instruments: MIRS or OROCHI, a spectrometer and optical chromatic imager.

Figure 1 - (left) Phobos and (right) Deimos, the two Martian moons. There are among the darkest Solar system objects. Phobos is characterized by a red unit on most of its surface and a bluer one near the Stickney crater. It is heavily cratered while Deimos has a smoother surface. (Image credit: NASA).

1.1. PHOBOS AND DEIMOS THROUGH PREVIOUS SPACE MISSION EXPLORATION

Phobos and Deimos are the only terrestrial planet satellites besides the Moon. Their origin has not yet been established and understanding their composition and geological evolution will provide information about the earliest stages of terrestrial planet formation (Michel, DeMeo, and Bottke 2015).

Compared to the Earth's Moon, the ones of Mars are quite small: Phobos has a diameter of 22.3km and Deimos is about 12.6km. These two satellites are orbiting Mars respectively in 7.66 hours at a semi major axis of 9.377km and in 30.35 hours at a semi major axis of 23.436km. The two moons are tidally locked and always present the same face to Mars as the Moon does to Earth. Phobos orbital radius is decreasing over time and when it will reach the Roche limit, it will either crash on Mars or form a ring.

These fates may have been the results of several moons before Phobos as described in The asteroid capture scenario part.

Phobos has been visited by the spacecraft Mariner 7 which provided the first image of the satellite. Following it, Mariner 9 established approximate dimensions of the two moons and shown resolving surface features such as their heavily cratered surfaces, low albedo[7] and covered by regolith[8]. There are among the darkest objects of the Solar system (Michel, DeMeo, and Bottke 2015). The Viking 1 and Viking 2 orbiters have provided higher resolution imaging from closer flybys of the moons. It is still the physical geology reference for our current knowledge. Phobos presents rough topography as crater, the biggest one being Stickney with 9.4 km diameter, and an irregular shape (Thomas 1979). Its albedo is as low as those of asteroids thought to have carbonaceous compositions. The reflectance varies spatially, and crater rims are covered by a brighter material, identified as the blue unit. In comparison Deimos has smoother surface with crater that are more degraded and infilled by regolith. Its surface reflectance is closer to the darker areas of Phobos, identified as the red unit. The spectrum obtained with the Mariner 9 and Viking missions revealed a flat spectrum at wavelength longer than 0.4 μm (Kuramoto et al. 2022).

More recently, CRISM[9] hyperspectral imager onboard Mars Reconnaissance Orbiter (MRO) spacecraft provided reflectance spectra of both Phobos and Deimos during one of its approaches to reach Mars orbit. The instrument is covering the visible and mid infrared ranges from 0.36 to 3.92μm with a resolution of 6.55nm/channel (Murchie et al. 2007). Its analysis is spread over two high resolution spectrometers: one is used for the visible/near-infrared channel (from 0.36 to 1.0μm) and the second one is for the infrared channel (from 1.0 to 3.92μm). It acquires three Martian moons observations in succession on 23rd of October 2007 with a phase angle of 41° and a spatial sampling of 350m/pixel. (Figure 2) (Fraeman et al. 2012; Fraeman and Nakamura 2023). CRISM instrument from the MRO mission has obtained spectra of both Phobos red and blue units. These unit have respectively a redder and bluer sloped spectrum. These spectra are relatively flat and do not present noticeable features except for the 2.71μm band which can be distinguished.

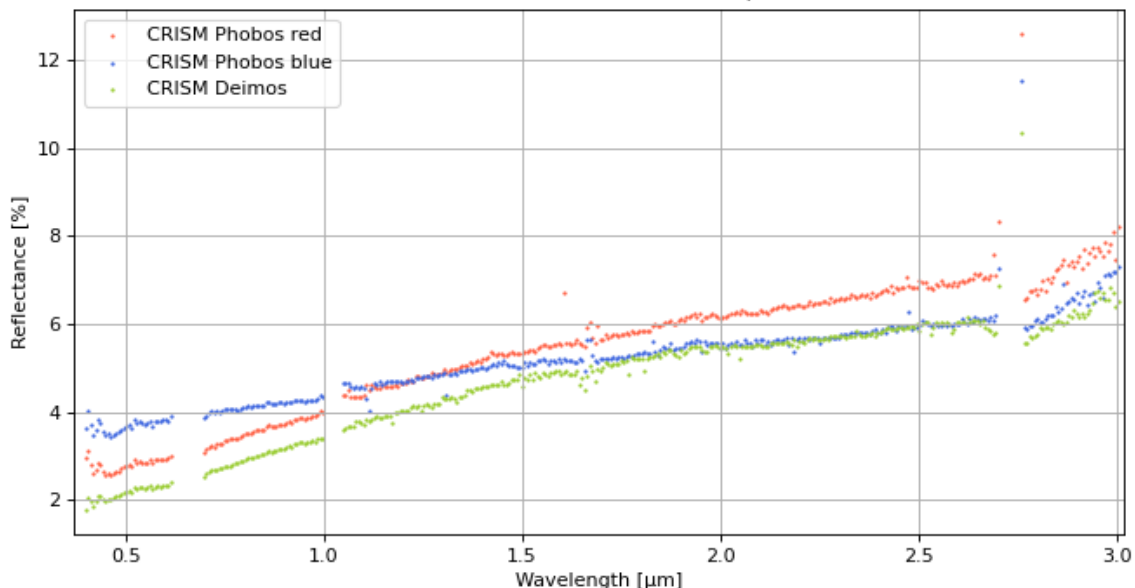Figure 2 - Phobos and Deimos reflectance spectra from CRISM data onboard MRO mission. Observations of the 23rd of October 2007 with a phase angle of 41° and a spatial sampling of 350nm/channel.

---

[7] Fraction of light reflected or diffused by a non-luminous body.
[8] Layer of unconsolidated solid material covering the bedrock of a planet.
[9] Compact Reconnaissance Imaging Spectrometer for Mars

1.2. ORIGIN HYPOTHESIS

The origin of Phobos and Deimos is still under discussion and two mains scenario are likely to explain the current Martian system: the giant impact and asteroid capture scenarios.

1.2.1. THE GIANT IMPACT SCENARIO

The giant impact scenario is similar to the formation of the Earth's Moon. In this scenario, Phobos and Deimos are the result of a collision between proto-Mars and an impactor of one-third its size. The material from the impactor would have been mixed with the Martian mantle and ejected into the planet's orbit. One derived hypothesis supposes the existence of additional bodies after the impact event. Indeed, the estimated mass of impact ejecta would have been much larger than that of both moons. During the impact, the debris would have coalesced into larger bodies and more than two bodies would have formed. Due to tidal interactions, these bodies would have fallen onto Mars, leaving the two smallest bodies (Phobos and Deimos) with near circular and near equatorial orbits in the corotation radius of Mars. Following this pattern, Phobos gets closer to its host planet every year. This hypothesis must be confirmed by geological evidence of the mass loss of a large moon onto the Martian surface (Kuramoto et al. 2022).

In order to assess such a scenario, it is possible to look at the composition of the soil. The moon surface composition should then be a mixture of proto-Mars materials such as silicate reservoirs and impactor materials (Hyodo et al. 2017; Canup and Salmon 2018). The endogenous Phobos materials should contain evidence of high-temperature and high-pressure shocked phases due to the impact. These phases could be pyroxene, olivine or evolved igneous rocks (Usui et al. 2020).

According to this scenario, studying Phobos and Deimos would provide information of the Martian mantellic composition, which is currently not reachable by digging into the planet surface. The composition analysis of Phobos and Deimos should give details over the giant impact phenomenon and planetary formation, as the composition is a recording of the geological history of the rock.

This hypothesis is still controversial to date. It remains unclear how such materials as proto-Mars and impactor materials lead to the current reflectance spectra of Phobos and Deimos. Moreover, this theory implies scenario similar to the Earth's Moon formation. The irregular shape of the Martian moons is unusual compared to the spherical shape this satellite. These two main points of controversy have opened the discussion to other theories such as asteroid capture.

1.2.2. THE ASTEROID CAPTURE SCENARIO

In the asteroid capture scenario, Phobos and Deimos would be two primitive bodies that would have been captured by Mars through tidal effects during the planetary migration period of the Solar system. The bodies could be originated from outer[10] or inner[11] Solar system.

In the case of an outer Solar system body, the endogenous materials should be rich in oxidized hydrous alteration phases such as phyllosilicates or carbonates, rich in volatiles and contain primitive organics. To study such origin hypothesis, reference studies can be operated over analogues as carbonaceous chondrites or interplanetary dust particles. Whereas for an inner Solar system body, the components should be anhydrous phases such as pyroxene, olivine, or sulphides and volatile poor (Usui et al. 2020). The analysis of the two moons will yield both clues on their formation and evolution and on the Mars formation and history.

Investigation on this hypothesis is supported by primitive bodies analogues such as Ryugu asteroid. This body is a dark object that is classified as a CB-type asteroid. Its composition and origin are fitting

---

[10] After the snow line. The snow line is the distance from the Sun at which water ice begins to sublimate.
[11] Before the snow line.

with the asteroid scenario materials and can be used as reference for this study. This asteroid has been visited by Hayabusa 2 mission which return 5.4g samples of Ryugu surface[12] and subsurface[13] for further studies in laboratory. These analyses provide precious information about its mineralogical and physical properties.

This second hypothesis is also controversial to date because of two phenomena: the dissipation of the initial orbital energy of the two moons and their low orbital inclinations and eccentricities. In the first case, the moons are heliocentric bodies. Their orbital energy must have been dissipated during their approach from Mars in order to be captured into its orbit. Tidal dissipations are too weak to face it alone but can be possible if the approaching velocity is near zero, which is unrealistic (Kuramoto et al. 2022). Some research suggest that such an event could have happened in the solar nebula gas. On the other hand, the orbital parameters of the Martian moons are unusual for bodies approaching from random directions, as observed with the satellites of the giant planets. For bodies approaching with a larger inclination, the tidal interactions with Mars are not strong enough to reduce it (Hunten, n.d.).

1.3. MMX - MARTIAN MOONS EXPLORATION MISSION

The uncertainties around the Martian moons' formation led the NASA and the JAXA to develop the Mars Moons eXploration mission. It will analyse the whole Martian system including Phobos, Deimos and Mars itself. MMX will be launch in 2024 and return Phobos surface samples to Earth in 2029. The opportunity to study direct samples from the surface will be a real breakthrough in the understanding of these moons. The mission has been designed to answer two major objectives (Usui et al. 2020):

   i)   Investigate over the origins of Martian moons, processes of planetary formation and material transport in the solar system,
   ii)   Observe the driving mechanism of Mars-moons system and learn more about the evolution history of Mars.

These questions will be investigated as the MMX mission is the first sample return mission from the Martian system. It is supported by numerous instruments which will provide data based on imagers, spectrometer, mass spectrum analyser, dust monitor, gamma ray analysis, lidar method and a rover (Kuramoto et al. 2022). Two of them are particularly relevant for this study: the infra-red spectrometer MIRS and the optical radiometer OROCHI. Both instruments will provide a near global mapping of reflectance spectra of Phobos. Their covered range will allow the detection of the 2.7-2.8μm band caused by hydroxyl group. This band position is various due to the Fe-Mg composition of the hydrous silicates.

The MIRS [14] instrument will provide a global spectral characterization of the moons and its measurements will be used both for origin determination and surface study for the sample collection sites. It ranges from 0.9μm to 3.6μm in wavelength range with a resolution smaller than 20nm (Barucci et al. 2021). This range will highlight the 2.7-2.8μm band that is lacking in the previous reflectance data of Phobos surface. Thanks to the MIRS data, hydrous materials and other related minerals should be identified. Moreover, the sampling site spectral characteristics should be analysed in a radius of 50m or more around the precise point.

Additionally, the spectral analysis will be supported by the OROCHI[15] instrument. It possesses seven wide angle bandpass imagers and a monochromatic imager dedicated to the observation of sample collection area. Its analysis will be combined to MIRS data to select the two more interesting points to collect the Phobos surface samples. OROCHI is working on seven bands for spectroscopy. The band

---

[12] Touchdown number 1 : undisturbed surface.
[13] Touchdown number 2: with excavated materials.
[14] MMX InfraRed Spectrometer.
[15] Observation of surface Reflectance by Optical Chromatic Imager.

centres are: 0.39, 0.48, 0.55, 0.65, 0.73, 0.86 and 0.95µm, with their band widths respectively being 0.05, 0.03, 0.03, 0.04, 0.04, 0.04 and 0.06µm. The details are also described in Table 3. Five of these seven bands have been determined according to ONC-T instrument onboard Hayabusa 2 mission. The two other ones, 0.65 and 0.73µm have been selected to characterize the absorption around 0.65µm, specific Phobos red unit feature (Fraeman et al. 2014; Kuramoto et al. 2022).

In addition, MIRS and OROCHI will contribute to analyse the Martian atmosphere with a particular attention to local time variation and climate (Kameda et al. 2021). Independently of sample analysis, the data will assess the Martian moons origin hypothesis and documents the sampling site to inform the geological context.

2. SAMPLES AND METHOD

2.1. UTPS - UNIVERSITY OF TOKYO PHOBOS SIMULANTS

To prepare the landing of the MMX mission, the science team needs to provide information such as the mechanical properties of the surface to the engineering team in charge. These properties can be bearing capacity, bulk frictional coefficient, or granular material behaviour (Miyamoto et al. 2021). Such information can be obtained by doing direct experiments on rocks, and on that purpose Phobos simulants have been developed by the University of Tokyo. Three UTPS[16] analogue rock samples have been created to answer different conditions and situations: Tagish Lake based (TB), impact based (IB) and simpler version (S).

2.1.1. IMPACT THEORY BASED SIMULANTS (UTPS-IB) AND SIMPLER VERSION (UTPS-S)

UTPS-IB is based on the impact scenario of Martian moons origin described in The giant impact scenario part. Its composition has been designed based on debris materials originated from the Martian crust and upper mantle mixed with asteroid materials (Miyamoto et al. 2021). UTPS-TB has been mixed with basalt and dunite to represent the asteroid material, Martian crust and Martian mantle materials, respectively.

UTPS-S has been designed to complete the IB and TB simulants, these last ones being very dark and fragile. To attend engineering test, a simpler version has been developed. Its mechanical properties have been favoured over spectral and optical properties. UTPS-S are mainly composed of serpentinite [17], dunite [18], silica sands, pyrites, magnetites, dolomites, calcites and phyllosilicates (Miyamoto et al. 2021). These simpler simulants have three sub-simulants varying on material ratios.

2.1.2. TAGISH LAKE BASED SIMULANTS (UTPS-TB)

2.1.2.1. TAGISH LAKE METEORITE

Tagish Lake meteorite fell in 2000 in Canada. The pieces of this carbonaceous chondrite are dark grey to almost black in colour with small light-coloured inclusions (Brown et al. 2000). Tagish Lake is composed of abundant phyllosilicate-rich matrix (~80%) and lesser amounts of carbonates, olivine, sulphides, and magnetite, sparse CAIs and aqueously altered chondrules (Alexander et al. 2007). This meteorite shows some similarities with the most primitive carbonaceous chondrite CI and CM types but still presents some distinct aspects. It has been classified as a C2 chondrite, but this ranking is still being discussed. Its more precise percent proportion has been described Table 1.

The CI (Ivuna-like) carbonaceous chondrites are among the most primitive ones and are corresponding to the less thermally altered. Their composition is characterised by a high abundance in volatile elements, as water or organic carbonates. Their isotopic composition, particularly for oxygen isotopes, is similar to that of the Sun, indicating that they have undergone very little alteration since their formation.

The CM (Mighei-like) carbonaceous chondrites are rich in organic carbon and hydrous minerals. They contain phyllosilicates, as serpentinite and smectite, which are indicators of the prolonged action of water in the parental bodies. CM-type carbonaceous chondrites generally undergo a moderate degree of thermal metamorphism.

The Tagish lake meteorite is one of the best analogue materials from the similarity in the reflectance spectra of Phobos (Cloutis et al. 2012).

---

[16] University of Tokyo Phobos Simulants.
[17] Olivine rich material.
[18] Olivine rich material.

2.1.2.2. THE UTPS-TB SAMPLE CHARACTERISTICS

These simulants are part of the asteroid capture theory and have been developed based on Tagish Lake meteorite composition. Without being identical, these two materials contain almost the same components as seen in Table 1. They need to be handling with a special care. Indeed, they can easily absorb water vapor and can stay fixed on instruments and hands.

Table 1- Mineral composition of Tagish Lake meteorite and UTPS-TB simulants.

Minerals	Tagish Lake (Cloutis et al. 2012)		UTPS-TB simulant (Miyamoto et al. 2021)	
	Details	Proportion [wt%]	Details	Proportion [wt%]
Phyllosilicate	Saponite-serpentinite Talc	60.3	Mg rich phyllosilicates Asbestos-free serpentinite	60.5
Olivine	Olivine	7.9	Mg rich olivine Dunite	7.3
Magnetite	Magnetite	8.3	Powdery magnetite	7.7
Sulphide	Pyrrhotite Pentlandite	9.1	Fe-Ni rich sulphides Pyrite	9.2
Carbonate	Siderite Calcite Dolomite Fe-Mg rich carbonates	14.4	Fe-Ca-Mg rich carbonates Limestone	10.3
Carbon			Nanoparticles carbon	~5
Organic			Polymer organic materials	~1

The received UTPS-TB samples were mixed without grain size distinction. Six grains sizes ranges have been selected to separate the sample according to the following sizes: larger than 1mm, between 1mm and 250µm, finer than 1mm, finer than 250µm, finer than 125µm, finer than 53µm. These sizes have been selected for different reasons according to the state of the art around Phobos surface. The 1mm stage is to highlight the larger grains. The 250 and 125 µm stage are close to already existing models from a previous paper (Miyamoto et al. 2021). The 53µm range corresponds to the smaller sieves available and is to highlight the smallest grains of the surface. In the first place, the 75µm was selected to represent the supposed mean grain size of Phobos surface but the grains were underrepresented to be analysed.

Table 2 - UTPS-TB samples weight details. The given names correspond to the names used in the following.

Grain size [µm]	Larger 1000	Between 1000 and 250	Finer 1000	Finer 250	Finer 125	Finer 53
Name	more1	1btw250	less1	less250	less125	less53
Weight [mg]	91	93	87	85	82	78

The studied samples are presented in Figure 3 and their details are given in Table 2. There were contained in sample holder with dimensions 8mm diameter and 2mm depth. The samples have been tapped ten times except for the larger than 1mm that have been positioned by hand in order to fulfil the possible holes. The experiments have been handled in a clean room.

Figure 3 - UTPS TB samples analyzed with a grain size (a) larger than 1mm (b) between 1mm and 250µm (c) finer than 1mm (d) finer than 250µm (e) finer than 125µm (f) finer than 53µm. The rocks have been separated thanks to five sieves. The scale is represented under each sample.

2.2. THE FT-IR SPECTROMETER AND DATA TREATMENT

The spectrometer at Tohoku University is a VERTEX 70v. This spectrometer has different characteristics according to its functional range as described in Table 3. The range of the VERTEX 7v is covering the range from 0.38µm to 15µm, from visible to mid infrared ranges. Each are later numerically combined.

2.2.1. SPECTROSCOPY ANALYSIS AND CONDITIONS

The spectrometer requires different conditions depending on the wavelength range. The filter for the shorter wavelengths is used to cut off the larger ones. The manipulation protocol has been described in The experimental protocol part in Appendix.

The instrument conditions have been established fixing the footprint diameter around 5 mm on sample surface, an incidence angle of 30° and an emission angle of 0° according to the dimensions described in Figure 14 in Appendix. The spectrometer took 2048 scans of each sample and returned the average of them. Additionally, the experimental conditions were under 2hPa pressure and vacuum conditions in the sample room.

Range number	1	2	3	4
Wavelength range	0.38-0.56μm	0.55-1.1μm	1.05-2.7μm	2.65-15μm
Light source	Xenon lamp	Halogen lamp		Grover
Splitter	Quartz			KBr
Detector	Si Diode		MCT	
Standard	Spectralon		Infragold	
Filter	Hwat-absorbing filter		-	-
Coolant	-	-	Liquid N$_2$ (for MCT)	
Resolution	32cm^{-1}	16cm^{-1}	8cm^{-1}	4cm^{-1}

Several phenomena and elements have to be considered. First of all, the bigger the aperture is, the stronger the reflectance will be. The aperture should be selected according to the study conditions. In the case of this measurements, the goal is to compare the spectra to already existing data, the aperture cannot be too small to fit as much as possible to past mission instruments. Secondly, the shorter wavelengths are sensitive to the surface conditions and so, the focus. If the Spectralon focus and sample focus are different, slopes can differ in the shorter wavelengths. Moreover, a bigger grain can also affect these slopes and led to mis confusion.

For example, for the grains included between 1mm and 250μm, the phenomenon has been observed (Figure 12 in Appendix). Depending on the grain position, the slope was either increasing or decreasing for smaller wavelengths. In the case of the blue slope, the sample was in the configuration 1 from Figure 13 (in Appendix), that can be defined as specular reflectance conditions. The light majority is reflected in the last mirror, and the light is almost fully captured. Whereas for the second configuration from Figure 13, the grain is not flat, and the beam is divided in multiple directions. The reflectance is then fainter. In order to evaluate the most probable conditions during MMX measurements and represent the average values of it, the red spectra have been selected for the next studies.

2.2.2. DATA PROCESSING, NORMALIZATION AND SLOPE CALCULATIONS

The following correction had been applied to the raw spectra. After the analysis in four different ranges defined in Table 3, individual spectra have been divided by the corresponding Infragold and Spectralon standards. The second range has been identified as the most stable one because of its analysis conditions. All raw spectra have been calibrated on this second range following:

$$R_{i_{calibrated}}(x) = R_i(x) \times \frac{R_j(k)}{R_i(k)}$$

where R$_i$ $_{calibrated}$ defined as calibrated reflectance of the range i, x defined as the current wavelength, R$_i$ defined as reflectance of the range I, R$_j$ defined as reflectance of the range j and k defined as link wavelength.

Finally, the calibrated spectra have been multiplied by a calibration spectrum to remove the effect of Spectralon bias features on the ranges number one and two.

Spectral slopes are calculated by dividing the difference between the reflectance at b band (0.48μm) and x band (0.86μm) by the reflectance at v band (0.55μm) times the wavelength width. The equation is the following:

$$slope_{b-x} = \frac{R(x) - R(b)}{R(v)(x - b)}$$

where slope$_{b-x}$ defined as slope between b and x OROCHI bands, R defined as reflectance, x/b/v defined as OROCHI bands.

Normalization is a key operation in the pre-processing of spectral signals. The aim of this operation is to limit the effect of the sensors on the reading and interpretation of the data. There is no unified approach to this operation in the literature. In the following, two methods are detailed.

To perform normalization, the spectrum is scaled to achieve a unit reflectance for a characteristic wavelength. A first approach consists in choosing a specific wavelength of reference. It is defined as:

$$R_{norm}(x) = \frac{R(x)}{R(band)}$$

where R$_{norm}$ defined as normalized reflectance, R defined as reflectance, x defined as current position, band defined as normalisation value (here 0.55 and 2.5µm).

The second normalization corresponds to a scale by the reference spectra and a shift to the desired band normalisation. It defined as:

$$R_{norm}(x) = \frac{R(x)}{R_{ref}(x)} - R(band)$$

with R$_{norm}$: normalized reflectance, R: reflectance, R$_{ref}$: reflectance of the reference spectra, x: current position, band: normalisation value (here 0.55 and 2.5µm).

This second normalization has the advantage to scale the curves on the same factor, and so reduce the outlier error propagation. However, if a reference presents a variability, the following results would not be exploitable. Moreover, there is no arbitrary criteria to choose the reference spectra among all of them, which exploit the non-unicity of the normalization.

In the case of the second type of normalization (Figure 4), no noticeable change is observed with respect to the choice of the reference spectrum. The spectra have close appearance. For that reason, the first type of normalization has been selected for the study.
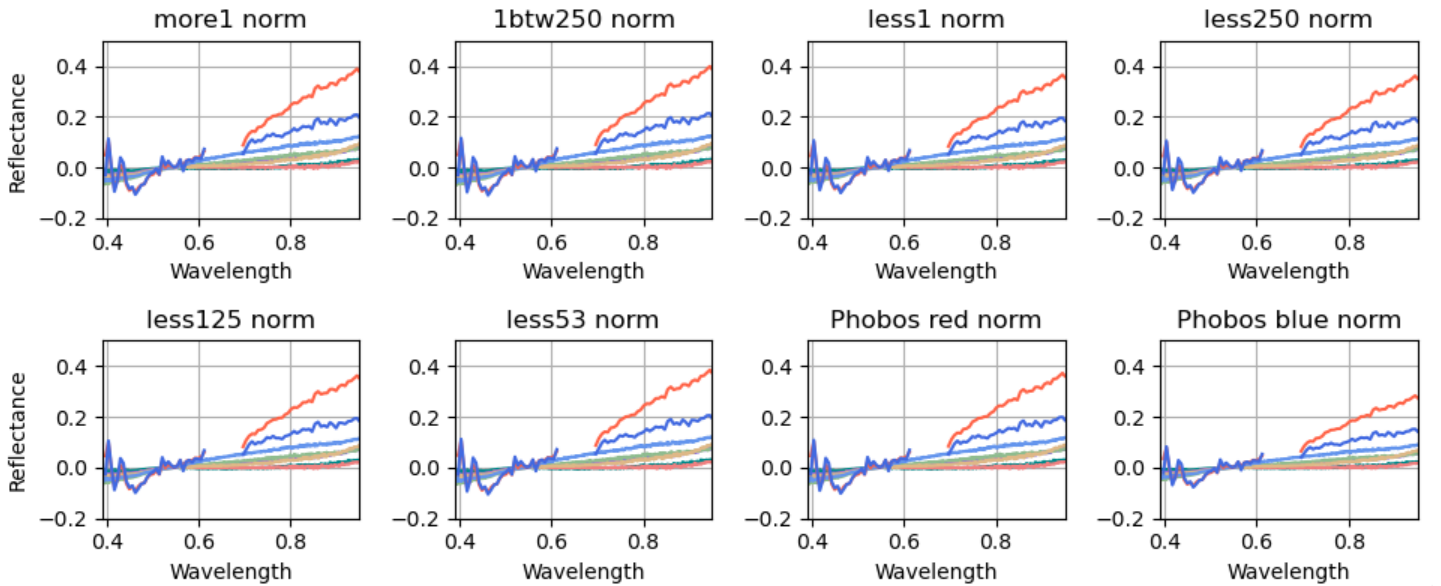

Figure 4 - Normalization by a reference spectrum (second type) according to different spectra of reference.

3.1. RYUGU MINERAL COMPOSITION

Two Ryugu asteroid samples have been analysed at Tohoku University on a FE-SEM/EDS[19], their reference names are: C0076-02 and C0025-03. The instrument operates on two modes: one of imaging and one of chemical analysis. The details of these two modes have been described in Appendix. On the imaging mode, the heavy elements are the brightest ones. As they contain many electrons, these last ones are reflected.

The major component of the first sample, C0076-02 (Figure 5 - 1), is phyllosilicates such as saponite and serpentine, which differ in Mg ratio. Carbonates, here dolomite, are the secondary components of Ryugu sample. The coarse bright particles are magnetite, formed due to aqueous alteration[20]. Magnetite is also present as framboid and plaquettes forms. These forms appear later in the mineral evolution. The brightest hexagonal shapes are pyrrhotite. The sample contains phosphate that has been removed (Figure 16 in Appendix) to determine its age. Finally, the sample has been formed in early Solar system history (Nakamura et al. 2023).

The C0025-03 sample (Figure 5 - 2) is composed of two blocks. The right one is the heavily altered one, which represents the major lithology[21] of Ryugu. The phyllosilicate is dominant as fine grains rich in Fe and S. There are also present as coarse grains of phyllosilicates. Some other elements can be identified such as magnetite and MgFe and MgCa carbonates (dolomite). The left part of the sample has been less altered (Figure 5 - 3). It also contains poorly crystallised phyllosilicates. Some particles have been formed at high temperature such as olivine and pyroxene. This sample composition has been studied through the element map (Figure 5 – 3 right) which described its full composition. In this sample, the dolomite is lacking and has been replaced by calcite due to the aqueous alteration rate (Figure 17 in Appendix) (Nakamura 2015).

Finally, depending on the aqueous alteration of the sample, Ryugu composition is slightly different. The major lithology of the asteroid is highly altered as the reflectance spectrum shows for the dolomite ratio in the major lithology sample part. Despite this divergence in the subcomponents, the major ones are phyllosilicates and carbonates. Ryugu mineral composition can be used as a reference for the mineral study of UTPS-TB simulants, based on asteroid capture scenario.

---

[19] Field-Emission Scanning Electron Microscope equipped with an Energy dispersive spectrometer.
[20] Change in composition of a rock, produced in response to interactions with H_2O-bearing ices, liquids, and vapors by chemical weathering (Bell, n.d.).
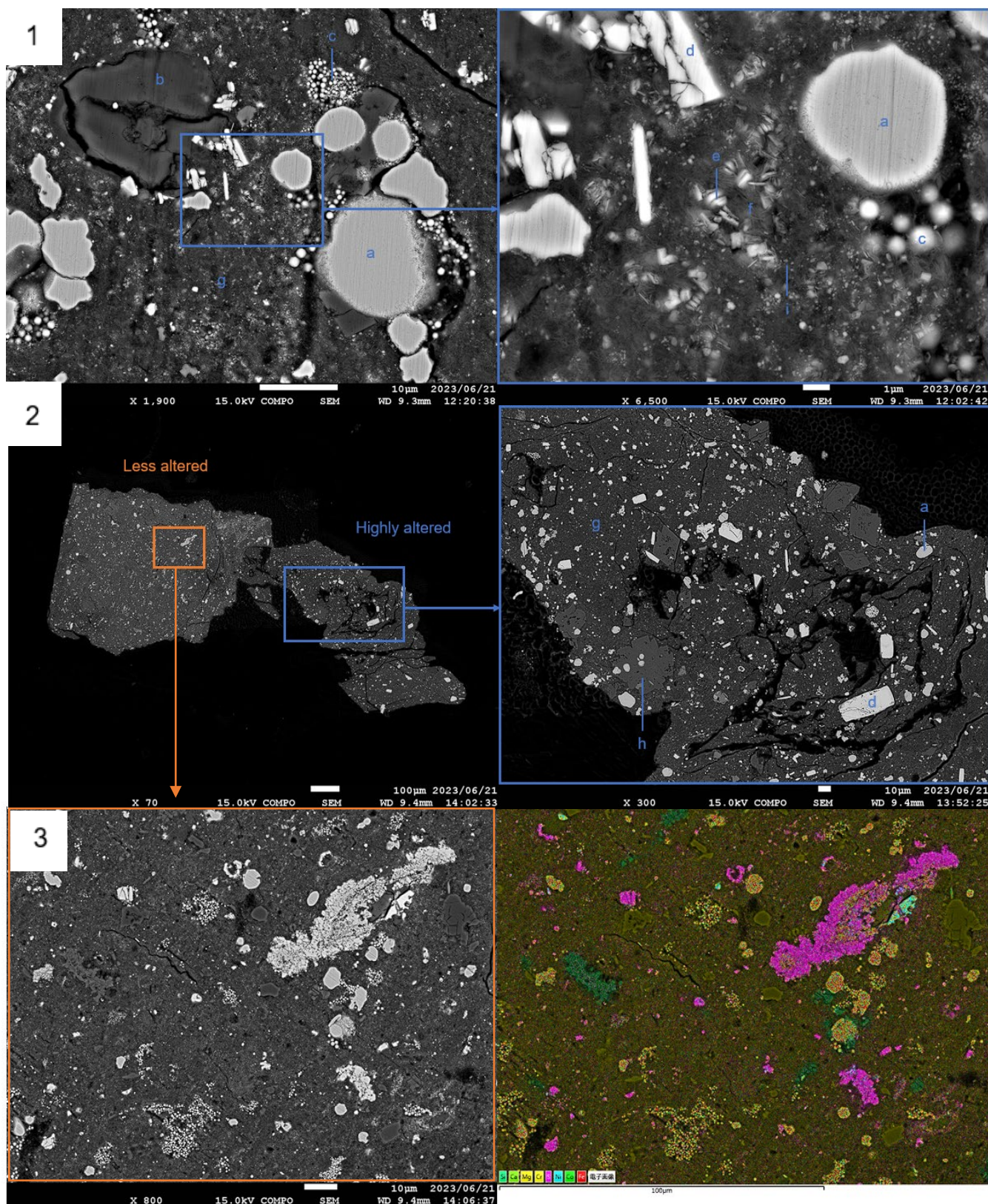[21] Study of the general physical characteristics of rocks.

Figure 5 – Ryugu (1) C0025-02 and (2)(3) C0076-03 samples mineral composition observed at FE-SEM/EDS. The elements are the following: (a) Magnetite, form from aqueous alteration (b) Phyllosilicates coarse grains (c) Magnetite framboid form (d) Pyrrhotite (e) Magnetite plaquettes form (f) Phyllosilicates plaquette form (g) Matrix of phyllosilicates (h) Dolomite coarse grains (i) Pentlandite + pyrrhotite. (3) left is the mineral composition of the less altered part of C0076-03 sample with (pink) Pyrrhotite (light blue) phosphite (green) pyroxene (dark green) calcite (yellow) magnetite.

18

3.2. PHOBOS SIMULANTS IN VISIBLE AND NEAR-INFRARED

The six UTPS-TB samples have been analysed on the four ranges defined in the Table 3. The resulting corrected spectra (Figure 6) are defined from 0.38 to 17.5µm which covers visible to near-infrared ranges.

These spectra present some important features that need to be defined. The observed peaks in the visible range are mainly due to electronics transitions whereas for near-infrared to infrared ranges, the band structure is affecting the peaks.

The 2.71µm peak translates a band stretching vibration between O-H connection. This hydroxyl group detection is due to the presence of phyllosilicates, that give information about aqueous alterations on the samples. This peak fits the mineral composition described in Table 1 as the phyllosilicates represents around 60% of the sample composition. Phyllosilicates presence can also be justified with the peak around 11.23µm, which corresponds to the Si-O⁻ stretching vibrations (Li et al. 2021). This peak gives additional information about the silicate's properties: if the peak is sharp, the phyllosilicates will be composed of perfect crystals, whereas for a larger width, it will correspond to a phyllosilicate low crystalline (amorphous). In the case of UTPS-TB, the middle case is privileged. The 16µm peak is also a translation for phyllosilicates presence. Additionally, the 9.1µm peak is a Christiansen feature and is induced by the concentration of SiO_2 in phyllosilicates in the powder. The position of the band peak at 9.1µm is resulting of a SiO_2 poor material (Giuranna et al. 2011).

Carbonates are responsible of numerous spectral peaks as they represent almost 10% of the sample composition (Table 1). This can be seen by the Ryugu spectra (Figure 7) and carbonates being one of its major components, its look can allow to identify TB simulants characteristics. The 3.4-3.5µm peak is a combination of carbonates and aliphatic group organics. The 3.95µm peak is carbonates characteristics (Bishop et al. 2021) and present, as in Ryugu powder, in the UTPS-TB samples.

Additionally to the mineralogical study, the reflectance dependence on the grain size can be noticed. The smaller the grains are, the higher the reflectance is. Moreover, it seems that for grain size between 53µm and 250µm the reflectance reaches a constant level according to the wavelength. The slope for smallest wavelengths also seems to depend on the grain size. For finest grains, the slope has a higher slope coefficient than for larger grains.

The UTPS-TB spectra obtained in laboratory are covering the OROCHI and MIRS ranges, MMX mission instruments, and a further study could allow to investigate on spectral features dependency on grain size.
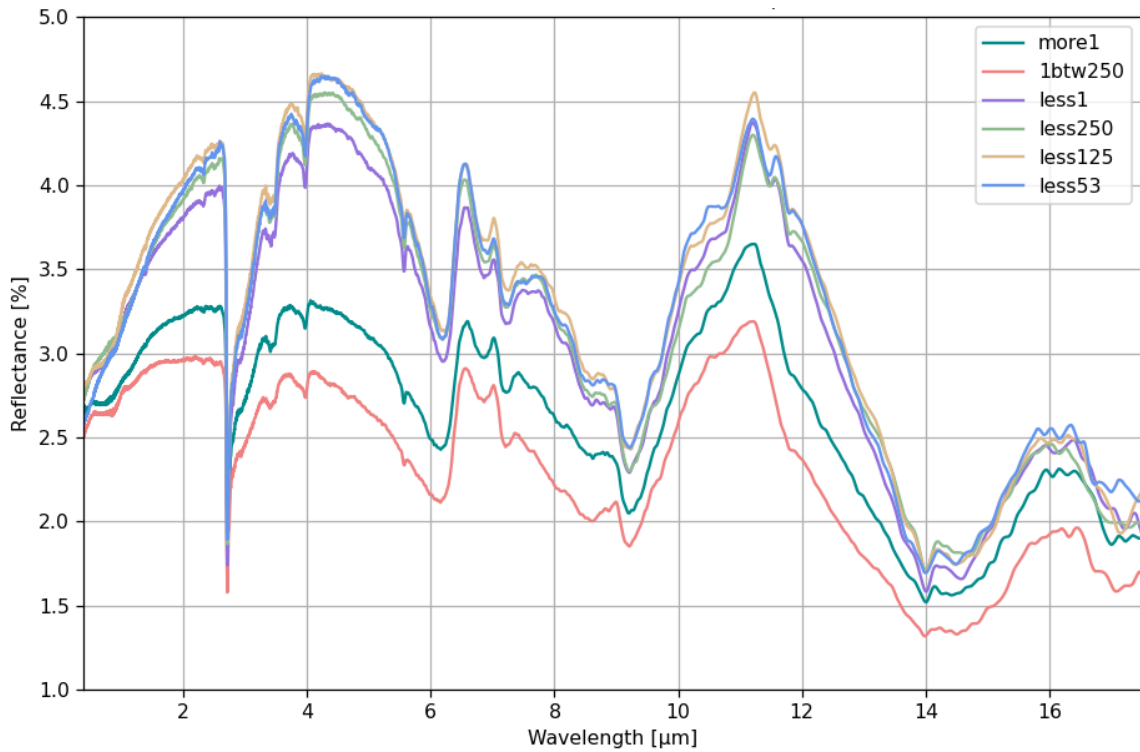
Figure 7 - UTPS-TB spectra in visible and near-infrared ranges. The spectra have been obtained by analysis on the VERTEX 70v FT-IR spectrometer and have been corrected by Infragold and Spectralon for each of the four ranges defined in Table 3.
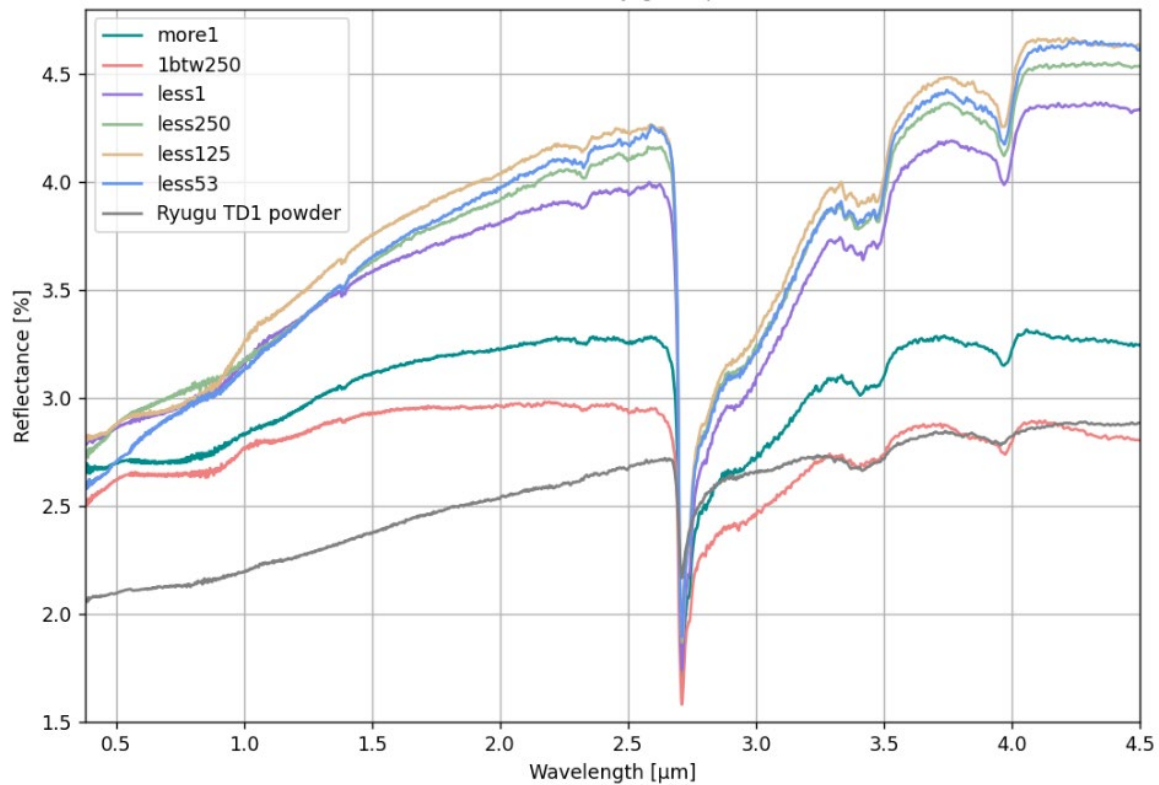

Figure 6 - UTPS-TB and Ryugu TD1 powdery sample reflectance spectra between 0.45 and 4.5μm. The Ryugu spectrum has been obtained from Tohoku University database.

The UTPS-TB spectra can be adapted to fit the MMX instruments characteristics in order to be compared to CRISM instrument data of MRO spacecraft. Analysing the simulants in the same conditions that CRISM data could confirm the validity of UTPS-TB samples as reference for Phobos surface and give evidence to support the asteroid capture hypothesis of Phobos origin.

The MMX instruments details have been defined in MMX - Martian Moons eXploration mission.

4.1. SIMULATION OF THE RESULTS IN OROCHI CONDITIONS

As described previously, the OROCHI instrument has been designed to operate on several specific bands defined in Table 4. Some of the ranges are based on the ONC-T instrument of Hayabusa 2 mission, their reference name has been used. Both of the seven bands of OROCHI have been added to detect a 0.65µm feature on Phobos spectra, these two additional bands are named *d* and *e*. The bands are covering from 0.39 to 0.95µm wavelength range. The instrument is giving the average value for each band over its specific band width.

Table 4 - OROCHI band details. The ranges have been named from letter a to g in order to make the reference easier. The ONC-T names for Hayabusa 2 mission have been given in parenthesis.

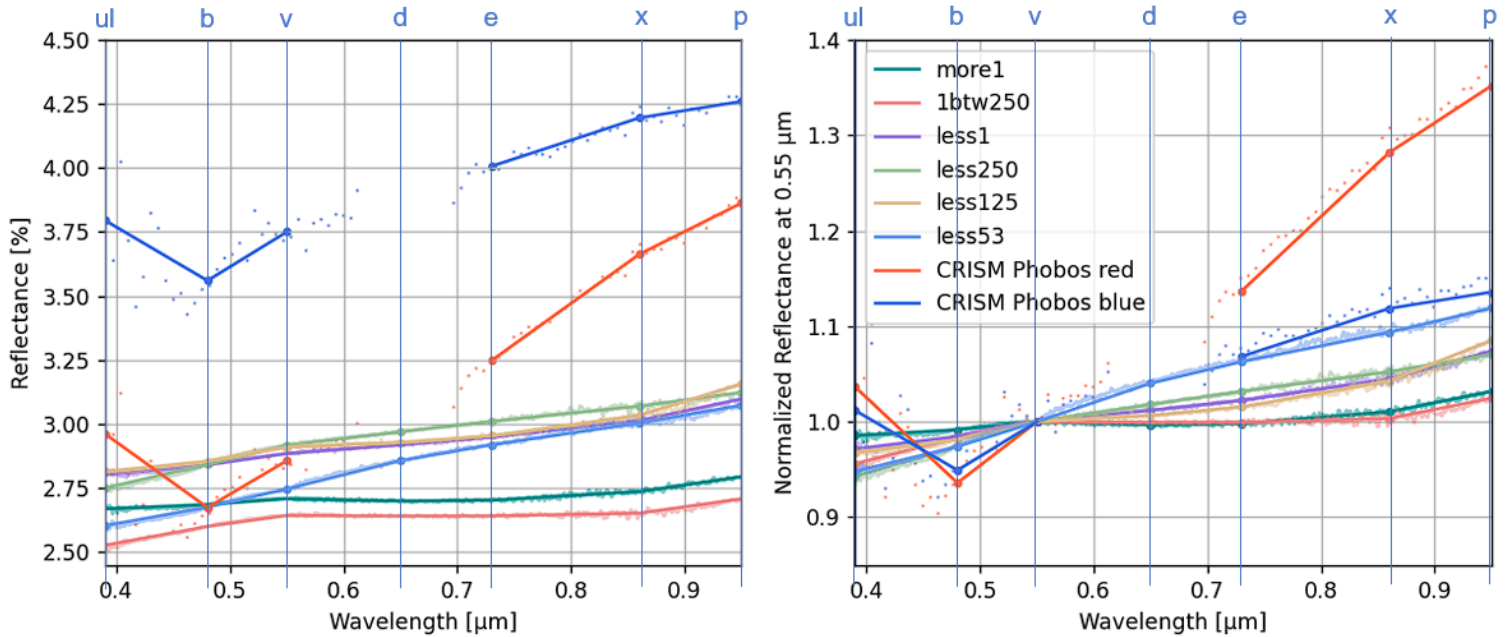| Band name	ul-	b-	v-	d	e	x-	p-
Band centre [µm]	0.39	0.48	0.55	0.65	0.73	0.86	0.95
Band width [µm]	0.05	0.03	0.03	0.04	0.03	0.03	0.06

Figure 8 - OROCHI conditions according to its filter bands for UTPS-TB and CRISM data. (left) Reflectance spectrum (right) Normalized reflectance at 0.55µm. The letters represent the band given in Table 4. The blurry signals are the raw signals from UTPS-TB and the straight lines are the average values obtained in OROCHI conditions.

Based on OROCHI conditions, the UTPS-TB samples and CRISM data have been processed to obtain the spectra of Figure 7. The spectra containing only the UTPS-TB samples have been uploaded in Figure 14 of Appendix.

The absolute reflectance is affected by mineral composition and organic concentration. With the same material, grainsize and porosity[22] affect the spectra. The compaction of finest grains is more difficult, so their porosity is usually higher than the one of larger grains at the surface. High porosity tends to reduce the absolute reflectance of powdery sample. In the case of the grains finer than 53μm, their reflectance seems to be smaller than the grains finer than 250 and 125μm. Grain size affects on both reflectance and slope, but porosity affects mainly on reflectance. Moreover, each sample has been tapped 10 times during the sample preparation which has as an effect to increase the porosity of the sample. According to this observation, the slope correlates better than the absolute reflectance to study the reflectance dependence on grain size.

The effect on slope appears to be more dominant for the finer sized particles than for the larger ones (Figure 9). In the case of Phobos study, the smallest grains have a redder slope whereas the bluer slopes are linked to the larger grains. To explain redder and bluer sloped spectra, the redder sloped spectra have a high reflectance for high wavelength, whereas bluer spectra have a higher reflectance for small wavelengths or a flatter slope. Moreover, it can be noticed that, in OROCHI bands, the reflectance grain dependence is respected to some extent, as the smallest grains have a higher reflectance value than the noticeable larger ones.

By comparing the b to x slope as a function of the reflectance at the normalized value 0.55μm (Figure 9), it can be noticed that the finest grains have a higher slope coefficient for b to x bands and a higher reflectance at 0.55μm. Based on this observation, the Phobos red and blue units should be smaller than 53μm, the smaller sieve selection from UTPS-TB studied samples. Their slope coefficient is even higher than the finest studied sample.
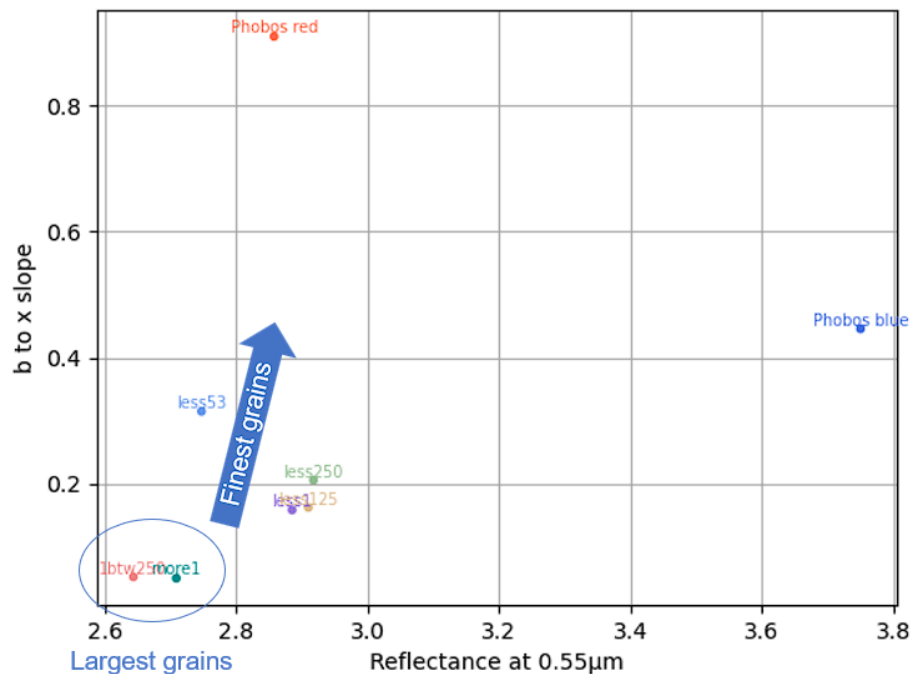

Figure 9 - b to x slope as a function to reflectance at 0.55μm. Each grain size and CRISM data have been named. Smallest grains present a higher b to x slope than larger ones.

---

[22] Void fraction in a sample, is included between 0 and 1.

4.2. Simulation of results in MIRS conditions

As described previously, the MIRS instrument is operating on the 0.9 to 3.6µm range with a 20nm resolution. In those conditions, the UTPS-TB samples and CRISM data have been treated to fit it (Figure 10).
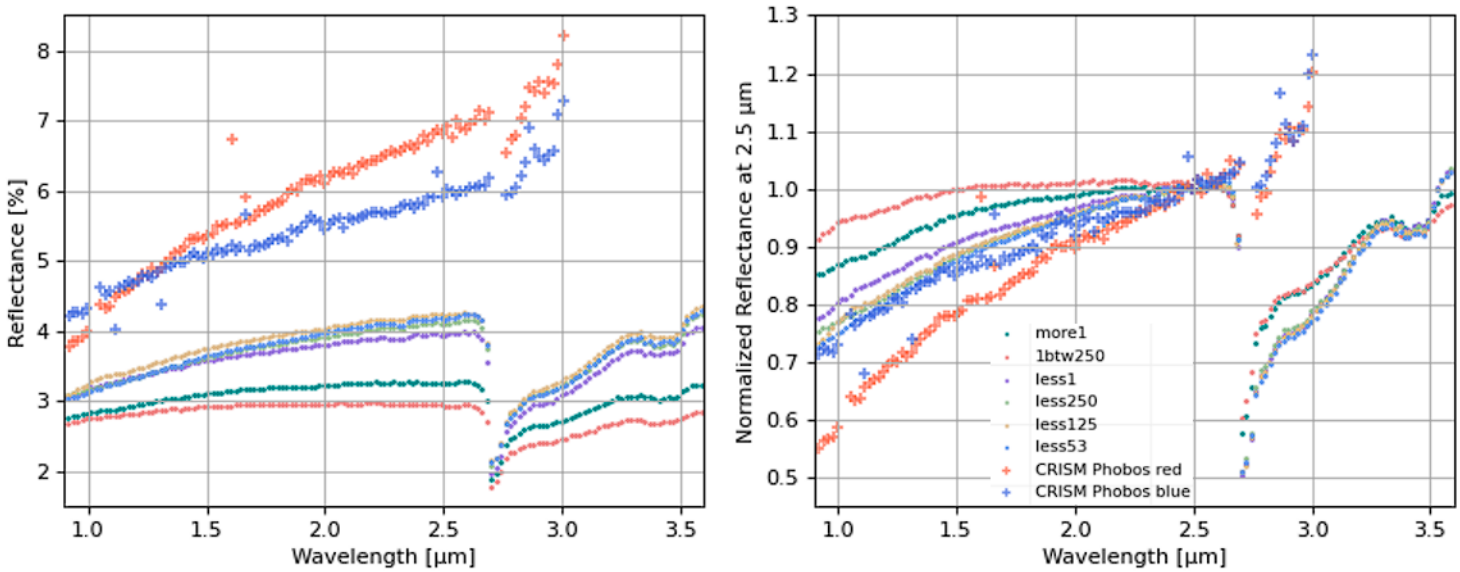

Figure 10 - MIRS conditions according to its resolution for UTPS-TB and CRISM data. (left) Reflectance spectrum (right) Normalized reflectance at 2.5µm.

Around 3µm Phobos CRISM data have been affected by thermal emission, which is not the case for UTPS-TB samples. In that extent, CRISM data had an increasing reflectance due to Phobos thermal emission which have been corrected on the data. As a solid body, Phobos captures thermal energy from the Sun and release it in infrared range. With its distance from the Sun, Phobos reflectance spectra is composed of thermal emission from Phobos surface and reflection of the Sun light (Figure 18 in Appendix). The peak wavelength for the black body radiation is obtained from Wien's displacement law:

$$2800 = X \times T$$

where X defined as peak wavelength of the thermal emission [µm] and T defined as temperature of the body [K].

In the case of Phobos, the surface temperature is varying between 300 to 218K approximately. Its peak wavelength of thermal emission is then around 10µm.

CRISM data have been corrected for this effect, whereas this correction seems to be not good enough to represent the 2.71µm phyllosilicates band. Two main reasons can explain this assumption. First, the spectra seem to be too much corrected before the band. Secondly, it is possible that CRISM instrument change its detector or filter in that range. Actually, the smallest wavelengths are not really affected by it and data are still consistent up to 2.5µm. In the conditions of OROCHI and MIRS instruments, the phenomenon can be considered in the analysis.

As demonstrate in previous section, the Phobos simulants contains the same materials as Phobos. Then the composition cannot explain the reflectance difference. The composition can actually slightly differ on their organics, such as their dark materials, in terms of quantity and composition. The UTPS-TB have actually been made darker than Phobos using a particular experimental method using dark materials (Miyamoto et al. 2021). Organics cause both a reflectance decrease and a masking effect in smallest wavelengths, that can erase the detection of others features (Giuranna et al. 2011). Depending

on its organic composition, the reflectance can be decreased (Figure 19 in Appendix). The organic composition of samples and Phobos surface can be a major reason of both featureless spectra and reflectance.

As described for OROCHI conditions, the slope is more consistent with the grain size analysis than the absolute reflectance itself. Additionally to the 1.0 to 2.5µm slope, the MIRS instrument contains the 2.71µm peak from phyllosilicates presence. For the CRISM data, this peak is not well represented because of a data lack. To consider it as precisely as possible in the current conditions, the depth has been calculated at 2.76µm for both CRISM and UTPS-TB data. This value corresponds to the closest available value at 2.71µm wavelength.

By analysing the relationship between the slope between 1.0 and 2.5µm and the band depth at 2.76µm to represent the band depth of the hydroxyl group peak (Figure 12), several points can be noticed.

The UTPS-TB samples are grouped according to their grain size. The finest ones have a high slope coefficient and a deep band at 2.71 µm. These features are smaller for the largest grains.

The slope coefficient seems to be higher for the finest grains but its band depth at 2.71µm is low compared to finest grains. The smaller grains seem to be dependent of a higher slope and a higher band depth. Whereas larger grains have a smaller slope coefficient for a smaller band depth at 2.71µm. Considering the Phobos CRISM data, whether for the red or blue unit, their slope is high as the finest grains but have a band depth close to zero. This can be explained as well by the band depth calculations at 2.76µm, which reduce the real band representation, and by the thermal emission explained before, which increases the band sides values.
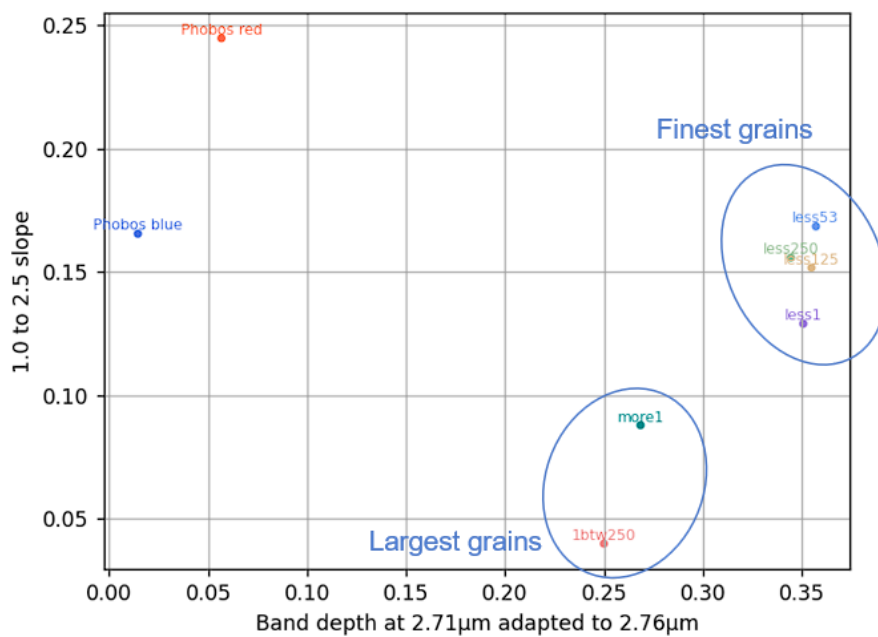

Figure 11 - Relationship between the slope from 1.0 to 2.5µm and the band depth at 2.71µm adapted to 2.76µm.

As another source of comparison, some simpler details of the spectra can be compared. By comparing the reflectance variation at the reference normalized values, 0.5 and 2.5µm (Table 5), it can be noticed that the CRISM data are almost fitting the UTPS-TB samples in OROCHI conditions. The values of CRISM instrument (2.0 to 3.5%) include the one of OROCHI (2.6 to 2.9%). However, in the MIRS conditions at 2.71µm, the absolute reflectance is much fainter than CRISM data. Once again, the thermal emission influences this range and can explain the larger reflectance for the CRISM data.

At 0.55µm	OROCHI	Phobos
Minimum reflectance [%]	2.9	3.5
Maximum reflectance [%]	2.6	2.0
At 2.5µm	MIRS	Phobos
Minimum reflectance [%]	4.2	7
Maximum reflectance [%]	3.0	5

4.3. THERMAL INERTIA APPROACH

The thermal inertia can characterise UTPS-TB simulants in another way than the absolute reflectance studied so far. The thermal inertia is depending on the grain size and porosity of the studied material. Finest grains make increase the temperature with a higher rate than the largest grains.

In the case of Phobos, its thermal inertia has been determined as 42.0 ± 13.6 J.m^{-2}K^{-1}s$^{-1/2}$ (Smith et al. 2018). According to the grain size correlation with the thermal inertia (Figure 13 left) the porosity of Phobos surface should be contained between 0.78 and 0.42 approximately, depending on the surface grain size.

The porosity has been calculated as following for the UTPS-TB samples:

$$Porosity = 1 - \frac{m}{v \times \rho}$$

where porosity defined as porosity of the sample, m defined as weight of the sample [g], v defined as volume of the holder compartment [cm^3] and ρ defined as grain density [g.cm^{-3}], here equals to 2.84 g.cm^{-3} (Miyamoto et al. 2021).

Finally, the six sample sizes are contained between 0.56 and 0.64 depending on the grain size (Figure 13 right). For those values, their thermal emission is close to 30 J.m^{-2}K^{-1}s$^{-1/2}$ (Figure 13 left). For the same particle diameter, the Phobos simulants are fitting the Phobos surface thermal inertia. This additional comparison confirm porosity cannot be a determining factor in the observed difference in reflectance.
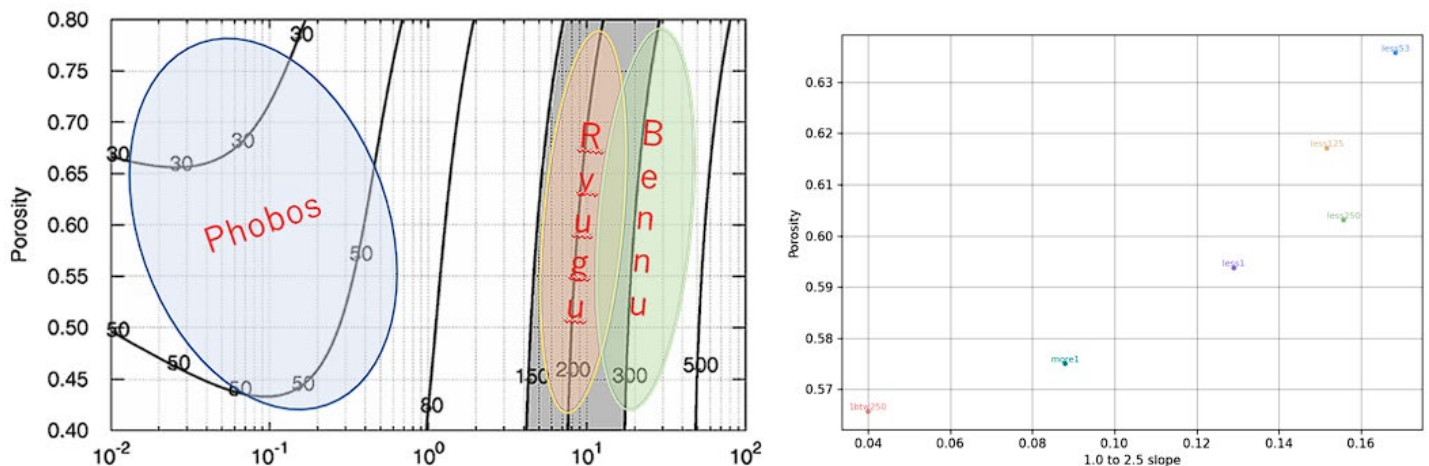

Figure 12 - (left) Grain size correlates with thermal inertia (right) Relationship between porosity and 1.0 to 2.0µm slope for UTPS-TB samples.

5. CONCLUSION AND DISCUSSION

Investigate on the Martian moon's origin will be supported by the MMX instruments MIRS and OROCHI in a few years. The University of Tokyo Phobos Simulants (UTPS) sub-versions as Impact Based (IB), Tagish Lake Based (TB) or Simpler version (S) allow the study of both giant impact and asteroid capture theories. Each of them has been created to fulfil a specific theory or objective. The TB version has been designed to support the asteroid capture scenario.

This study assumes that in those conditions, Phobos can be assimilated as a hydrated asteroid. Based on its nearly featureless spectrum in visible and near-infrared range, except for the 0.65 and 2.71μm features, its spectrum seems consistent with asteroid spectra as Ryugu one.

The comparison of Phobos, Phobos simulants and Ryugu spectra suggests that the three materials have similar overall spectral features and contains a major phase of phyllosilicates, a minor of carbonates and other materials as organics. Their reflectance spectra are classified as follows: Phobos is the brightest, UTPS-TB is medium and Ryugu is the darkest. Because of their similar composition, their reflectance variation could come from their dark material differences, in terms of quantity and composition. Organics cause both a reflectance decrease and a masking effect in smallest wavelengths, that can erase the detection of others features. The masking effect is less important in mid-infrared but Phobos surface reflectance data lacks in that range.

In addition to mineral composition and organic concentration, the absolute reflectance is affected by grainsize and porosity with same material conditions. Focusing on the porosity, finest grains have a higher porosity than larger ones and a higher porosity is usually reducing the reflectance. The thermal inertia of Phobos simulants, obtained from porosity, is fitting the Phobos thermal inertia for the same grain sizes and confirms that porosity is not responsible for the reflectance difference. Moreover, the difference between red and blue units of Phobos surface are not well understood. Their porosity being the same, the reflectance difference between these both units cannot be explained by it.

To analyse the grain size effect on Phobos spectra, a direct comparison between Phobos and TB simulants is required. Due to of their absolute reflectance difference, the spectra require normalization. After being processed, the UTPS simulants have shallower slopes in visible and near-infrared ranges compared to the red and blue units of Phobos surface. Smallest grains present a reddish slope and deeper band depth on reflectance spectra. The finding of a shallower slope for the samples would indicate grains finer than 53μm on the surface of Phobos. Moreover, the Phobos blue unit has characteristics similar to grains finer than 53μm. When the spectra are normalized to 0.55 and 2.71μm, the blue unit spectrum is almost fitting that grain spectral features.

The surface of Phobos faces space weathering, which is not the case for simulants. This phenomenon is changing the colour of the surface affected. The slope is getting bluer or redder according to the materials characteristics. For the Solar wind, the energy engaged is around 4keV, which have for effect to reddening and darkening the slope (Nakamura et al. 2015). The space weathering is probably to considered in the red and blue unit difference.

Finally, the detection of the hydroxyl group band feature around 2.71μm would strongly support the asteroid capture scenario as the scenario for Phobos and Deimos origin, as it is a main spectral features of asteroid reflectance spectra. However, with the current CRISM data, this peak cannot be confirmed due to the lack of information around that band. In that context, the MIRS instrument onboard MMX spacecraft will give precious information about the phyllosilicate's presence on Phobos surface.

6. ACKNOWLEDGMENTS

BIBLIOGRAPHY

Alexander, C.M.O'D., M. Fogel, H. Yabuta, and G.D. Cody. 2007. 'The Origin and Evolution of Chondrites Recorded in the Elemental and Isotopic Compositions of Their Macromolecular Organic Matter'. *Geochimica et Cosmochimica Acta* 71 (17): 4380–4403. https://doi.org/10.1016/j.gca.2007.06.052.

Barucci, Maria Antonietta, Jean-Michel Reess, Pernelle Bernardi, Alain Doressoundiram, Sonia Fornasier, Michel Le Du, Takahiro Iwata, et al. 2021. 'MIRS: An Imaging Spectrometer for the MMX Mission'. *Earth, Planets and Space* 73 (1): 211. https://doi.org/10.1186/s40623-021-01423-2.

Bell, Jim. n.d. 'Chapter 23: Aqueous Alteration on Mars'.

Bishop, J. L., S. J. King, M. D. Lane, A. J. Brown, B. Lafuente, T. Hiroi, R. Roberts, G. A. Swayze, J.-F. Lin, and M. Sánchez Román. 2021. 'Spectral Properties of Anhydrous Carbonates and Nitrates'. *Earth and Space Science* 8 (10). https://doi.org/10.1029/2021EA001844.

Brown, Peter G., Alan R. Hildebrand, Michael E. Zolensky, Monica Grady, Robert N. Clayton, Toshiko K. Mayeda, Edward Tagliaferri, et al. 2000. 'The Fall, Recovery, Orbit, and Composition of the Tagish Lake Meteorite: A New Type of Carbonaceous Chondrite'. *Science* 290 (5490): 320–25. https://doi.org/10.1126/science.290.5490.320.

Canup, Robin, and Julien Salmon. 2018. 'Origin of Phobos and Deimos by the Impact of a Vesta-to-Ceres Sized Body with Mars'. *Science Advances* 4 (4): eaar6887. https://doi.org/10.1126/sciadv.aar6887.

Cloutis, E.A., P. Hudon, T. Hiroi, M.J. Gaffey, and P. Mann. 2012. 'Spectral Reflectance Properties of Carbonaceous Chondrites: 8. "Other" Carbonaceous Chondrites: CH, Ungrouped, Polymict, Xenolithic Inclusions, and R Chondrites'. *Icarus* 221 (2): 984–1001. https://doi.org/10.1016/j.icarus.2012.10.008.

Fraeman, A. A., R. E. Arvidson, S. L. Murchie, A. Rivkin, J.-P. Bibring, T. H. Choo, B. Gondet, et al. 2012. 'Analysis of Disk-Resolved OMEGA and CRISM Spectral Observations of Phobos and Deimos'. *Journal of Geophysical Research: Planets* 117 (E11). https://doi.org/10.1029/2012JE004137.

Fraeman, A.A., S.L. Murchie, R.E. Arvidson, R.N. Clark, R.V. Morris, A.S. Rivkin, and F. Vilas. 2014. 'Spectral Absorptions on Phobos and Deimos in the Visible/near Infrared Wavelengths and Their Compositional Constraints'. *Icarus* 229 (February): 196–205. https://doi.org/10.1016/j.icarus.2013.11.021.

Fraeman and Nakamura. 2023. 'Phobos and Deimos Unpublished Data'.

Giuranna, M., T.L. Roush, T. Duxbury, R.C. Hogan, C. Carli, A. Geminale, and V. Formisano. 2011. 'Compositional Interpretation of PFS/MEx and TES/MGS Thermal Infrared Spectra of Phobos'. *Planetary and Space Science* 59 (13): 1308–25. https://doi.org/10.1016/j.pss.2011.01.019.

Hunten, M. n.d. 'Capture of Phobos and Deimos by Protoatmospheric Drag'.

Hyodo, Ryuki, Hidenori Genda, Sébastien Charnoz, and Pascal Rosenblatt. 2017. 'On the Impact Origin of Phobos and Deimos. I. Thermodynamic and Physical Aspects'. *The Astrophysical Journal* 845 (2): 125. https://doi.org/10.3847/1538-4357/aa81c4.

Kameda, Shingo, Masanobu Ozaki, Keigo Enya, Ryota Fuse, Toru Kouyama, Naoya Sakatani, Hidehiko Suzuki, et al. 2021. 'Design of Telescopic Nadir Imager for Geomorphology (TENGOO) and Observation of Surface Reflectance by Optical Chromatic Imager (OROCHI) for the Martian Moons Exploration (MMX)'. *Earth, Planets and Space* 73 (1): 218. https://doi.org/10.1186/s40623-021-01462-9.

Kuramoto, Kiyoshi, Yasuhiro Kawakatsu, Masaki Fujimoto, Akito Araya, Maria Antonietta Barucci, Hidenori Genda, Naru Hirata, et al. 2022. 'Martian Moons Exploration MMX: Sample Return Mission to Phobos Elucidating Formation Processes of Habitable Planets'. *Earth, Planets and Space* 74 (1): 12. https://doi.org/10.1186/s40623-021-01545-7.

Li, Jiangling, Feifei Lai, Mei Leng, Yangfan Chen, and Qingcai Liu. 2021. 'Effect of Cooling Rate on the Structure of CaO–SiO_2–CaF_2-Based Glassy Mold Flux'. *ISIJ International* 61 (5): 1532–38. https://doi.org/10.2355/isijinternational.ISIJINT-2020-423.

Michel, Patrick, Francesca E. DeMeo, and William F. Bottke. 2015. *Asteroids IV*. University of Arizona Press.

Miyamoto, Hideaki, Takafumi Niihara, Koji Wada, Kazunori Ogawa, Hiroki Senshu, Patrick Michel, Hiroshi Kikuchi, et al. 2021. 'Surface Environment of Phobos and Phobos Simulant UTPS'. *Earth, Planets and Space* 73 (1): 214. https://doi.org/10.1186/s40623-021-01406-3.

Murchie, S., R. Arvidson, P. Bedini, K. Beisser, J.-P. Bibring, J. Bishop, J. Boldt, et al. 2007. 'Compact Reconnaissance Imaging Spectrometer for Mars (CRISM) on Mars Reconnaissance Orbiter (MRO)'. *Journal of Geophysical Research* 112 (E5): E05S03. https://doi.org/10.1029/2006JE002682.

Nakamura. 2015. 'Unpublished Data'.

Nakamura, T, C Lantz, S Kobayashi, Y Nakauchi, K Amano, R Brunetto, M Matsumoto, et al. 2015. 'Experimental Reproduction of Space Weathering of C-Type Asteroids by He Exposure to Shocked and Partially Dehydrated Carbonaceous Chondrites'.

Nakamura, T., M. Matsumoto, K. Amano, Y. Enokido, M. E. Zolensky, T. Mikouchi, H. Genda, et al. 2023. 'Formation and Evolution of Carbonaceous Asteroid Ryugu: Direct Evidence from Returned Samples'. *Science* 379 (6634): eabn8671. https://doi.org/10.1126/science.abn8671.

Smith et al. 2018. 'Mapping the Thermal Inertia of Phobos Using MGS-TES Observations and Thermophysical Modeling'.

Thomas, Peter. 1979. 'Surface Features of Phobos and Deimos'. *Icarus* 40 (2): 223–43. https://doi.org/10.1016/0019-1035(79)90069-1.

Usui, Tomohiro, Ken-ichi Bajo, Wataru Fujiya, Yoshihiro Furukawa, Mizuho Koike, Yayoi N. Miura, Haruna Sugahara, Shogo Tachibana, Yoshinori Takano, and Kiyoshi Kuramoto. 2020. 'The Importance of Phobos Sample Return for Understanding the Mars-Moon System'. *Space Science Reviews* 216 (4): 49. https://doi.org/10.1007/s11214-020-00668-9.

APPENDIX

THE EXPERIMENTAL PROTOCOL

The experimentations have been separated over four days. Each session has been performed in a clean room. Here are the details for each step.

Setting the standard (Infragold)

Input of liquid nitrogen

Wait about 30 min

The measurement of Infragold (Range 4)

Changing splitters (KBr to Quartz)

Input of liquid nitrogen

Wait about 30 min

The measurement of Infragold (Range 3)

Changing splitters (Quartz to KBr)

Setting the sample and Spectralon

Input of liquid nitrogen

Wait about 30 min

The measurement of the sample (Range 4)

Changing splitters (KBr to Quartz)

Input of liquid nitrogen

Wait about 30 min

The measurement of the sample (Range 3)

The measurement of the Spectralon (Range 2)

The measurement of the sample (Range 2)

The measurement of the Spectralon (Range 1)

The measurement of the sample (Range 1)

REFLECTANCE DEPENDANCY ON GRAIN GEOMETRY

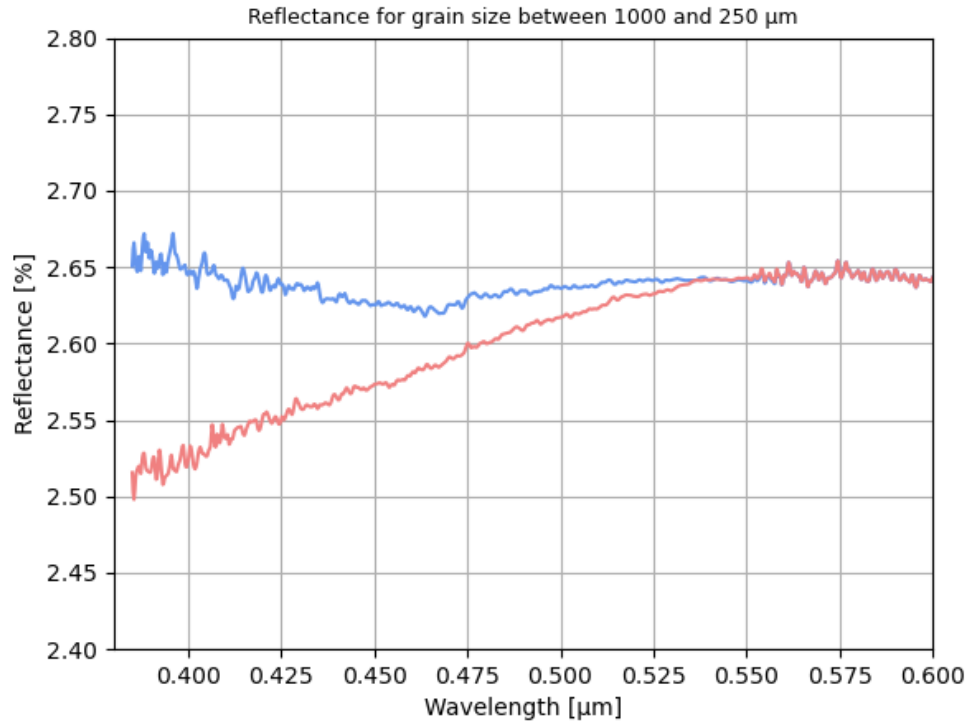Both figures are described in Spectroscopy analysis and conditions part.

Figure 13 - Reflectance dependance on grain geometry for grains between 1000 and 250µm. The red slope represents the average value for larger grains, in configuration 2 in Figure 12 . The blue slope represents the case of configuration 1 in Figure 12.
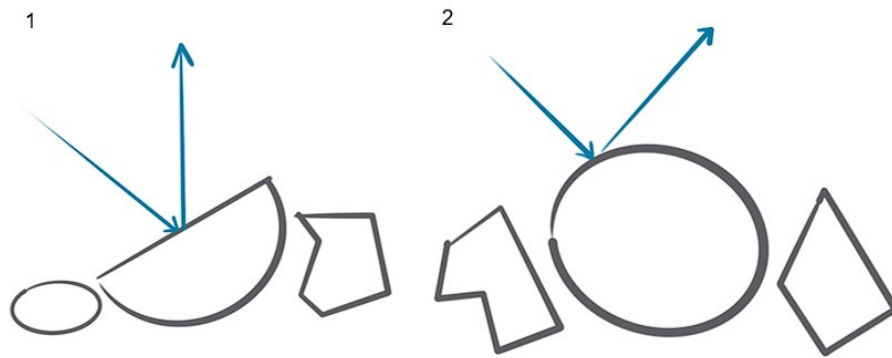

Figure 14 - Grain geometry configuration for spectrometry analysis. Both configurations are depending on the grain geometry for larger grains. Configuration 1 is the case of specular reflection, the beam is fully captured by the instrument. Configuration 2 is the case in which the beam is divided in different directions.

VERTEX 70v Spectrometer optic Layout

The Tohoku University spectrometer beam path is described as Figure 15.

The basic principle of an FTIR spectrometer involves the measurement of the absorption, transmission, and reflection of infrared light by a sample. It operates in the infrared region of the electromagnetic spectrum, which spans wavelengths longer than those of visible light.

The instrument consists of several key components. First, there is a source that generates infrared light. The light is then focused onto an interferometer, which splits the beam into two paths. One path travels directly to a reference mirror, while the other path is directed towards the sample being analyzed. After interacting with the sample, the light from both paths is recombined using the interferometer. This creates an interference pattern, the interferogram, which contains information about the sample's absorption and transmission properties at different wavelengths. Next, the interferogram is mathematically transformed using a Fourier transform algorithm. This process converts the interferogram from the time domain to the frequency domain, producing a spectrum known as the infrared spectrum. The infrared spectrum represents the unique fingerprint of the sample, as different functional groups and molecular structures absorb infrared light at specific frequencies.
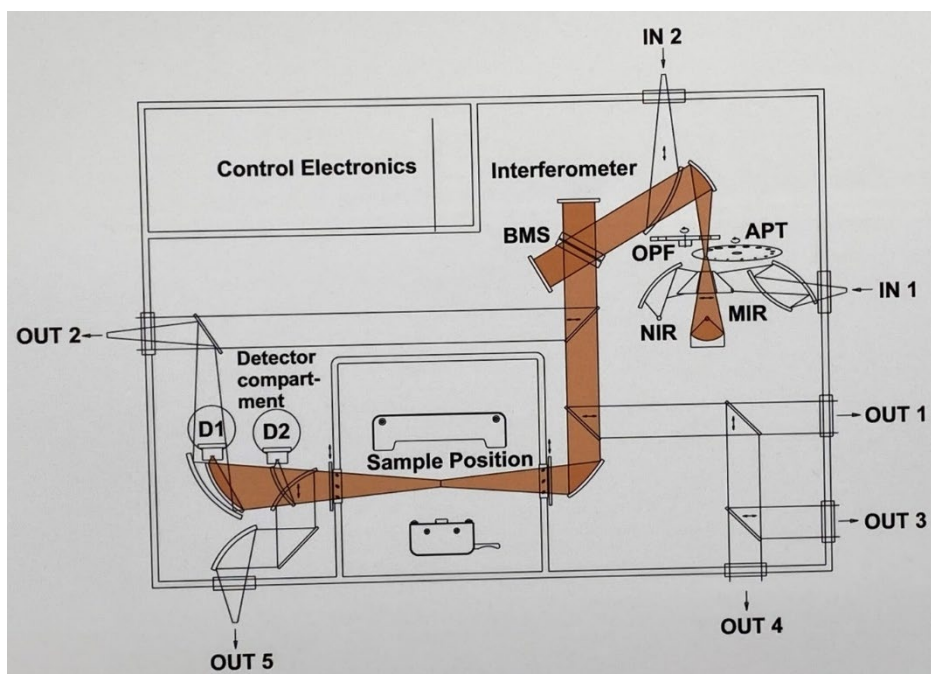

Figure 15 - VERTEX 70v optic layout.

Ryugu C0076-02 and C0025-03 samples observed with FE-SEM-EDS

These both samples have been analysed at the FE-SEM/EDS instrument. This instrument is working on two modes:

(i)   Imaging mode: the electron beam is projected on the whole sample. According to the sample composition, the electrons are reflected to give the black and white image which corresponds to the electron ratio of the materials. A heavy material, containing many electron, will reflect the beam faster and appear bright on the image. The darkest objects are then the lightest elements. This mode gives images such as Figure 16.

(ii)   Chemical analysis mode: the beam is concentrated on one area of the sample and measure energy coming out of the materials. To give enough energy to excites the electrons and detect the composition, the electron beam energy is around 15keV. This mode is giving information about the chemical composition of the material and provide spectra such as Figure 17.
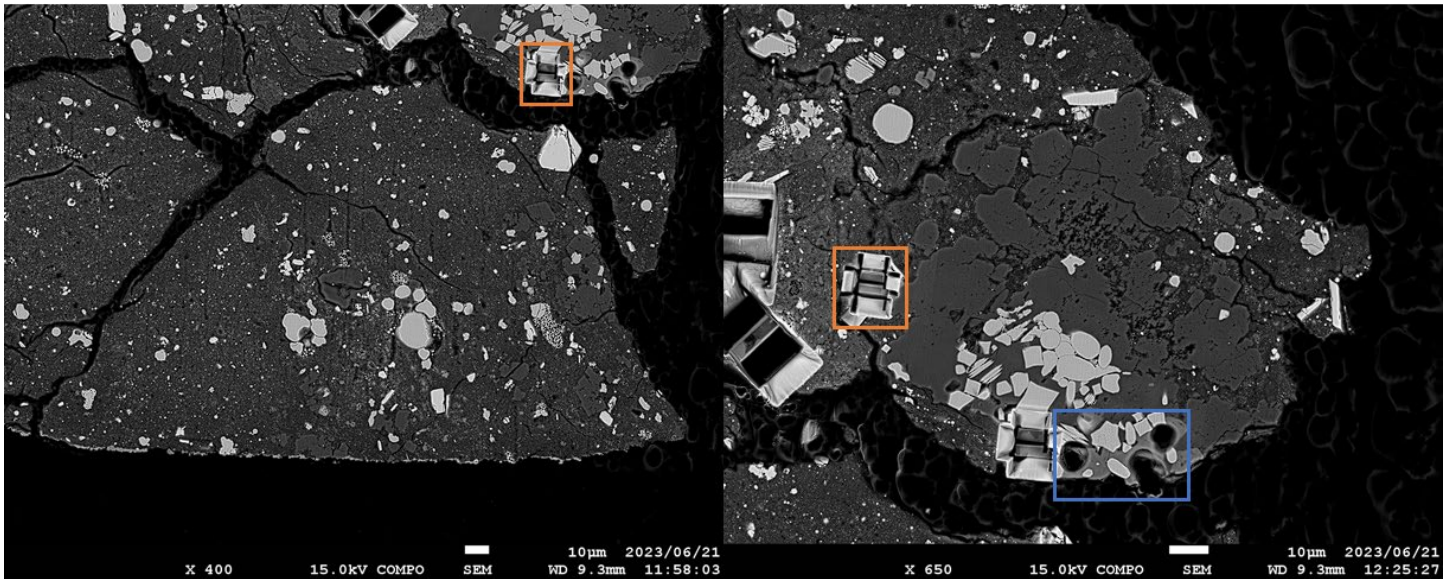

Figure 16 - Ryugu C0076-02 sample observed at FE-SEM/EDS at Tohoku University. The blue square corresponds to phosphate removal. Orange square corresponds to removal for synchrotron analysis.
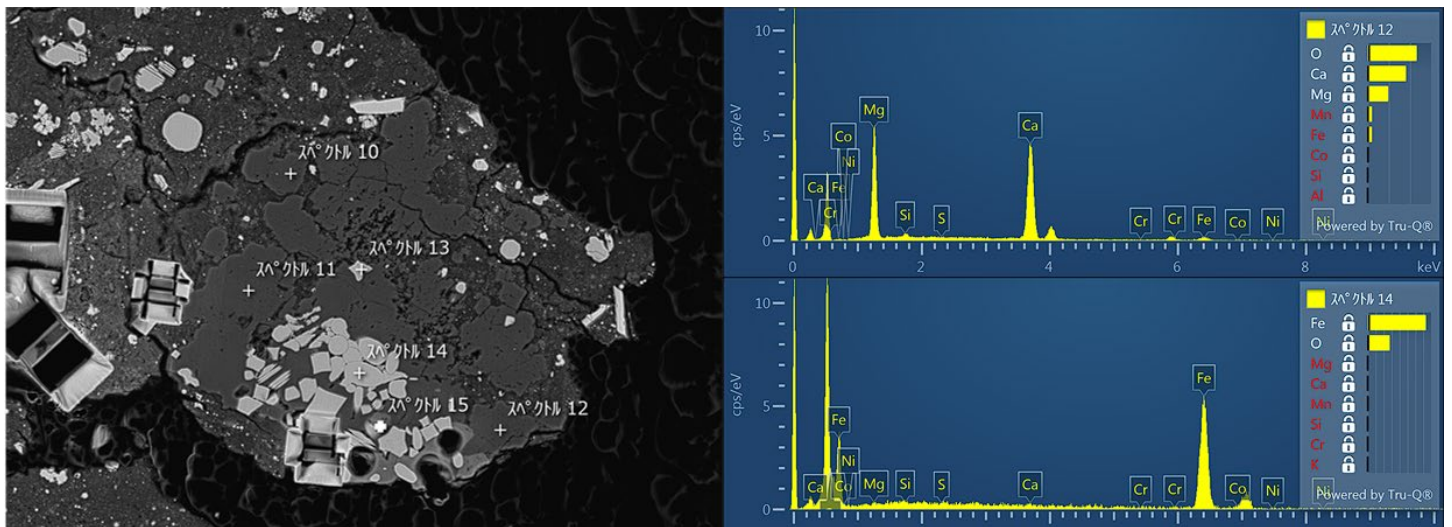

Figure 17 - Ryugu C0076-02 observed at FE-SEM/EDS. (right) Sample observed in first mode (left) chemical composition of the 12 and 14 points obtained with the second mode.

The following spectra is coming from (Nakamura 2015). It describes the aqueous alteration effect on rock components.
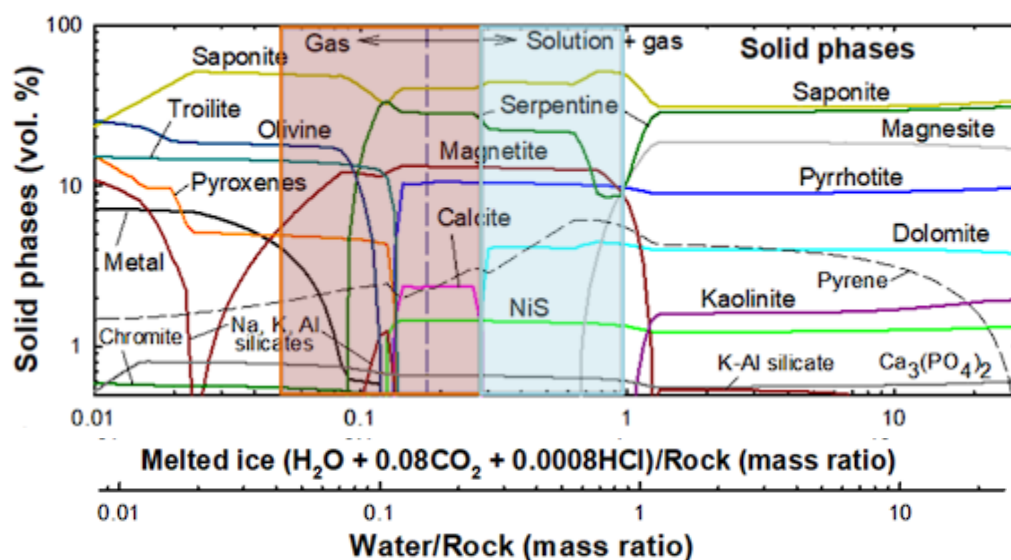

Figure 18 - Aqueous alteration conditions. The dolomite is dominant for high aqueous alteration, whereas calcite is dominant in a less aqueously altered rock.

UTPS-TB AND CRISM SPECTRA

The Phobos simulants UTPS-TB and CRISM data can be compared on Figure 18. The CRISM data have been provided by (Fraeman and Nakamura 2023).
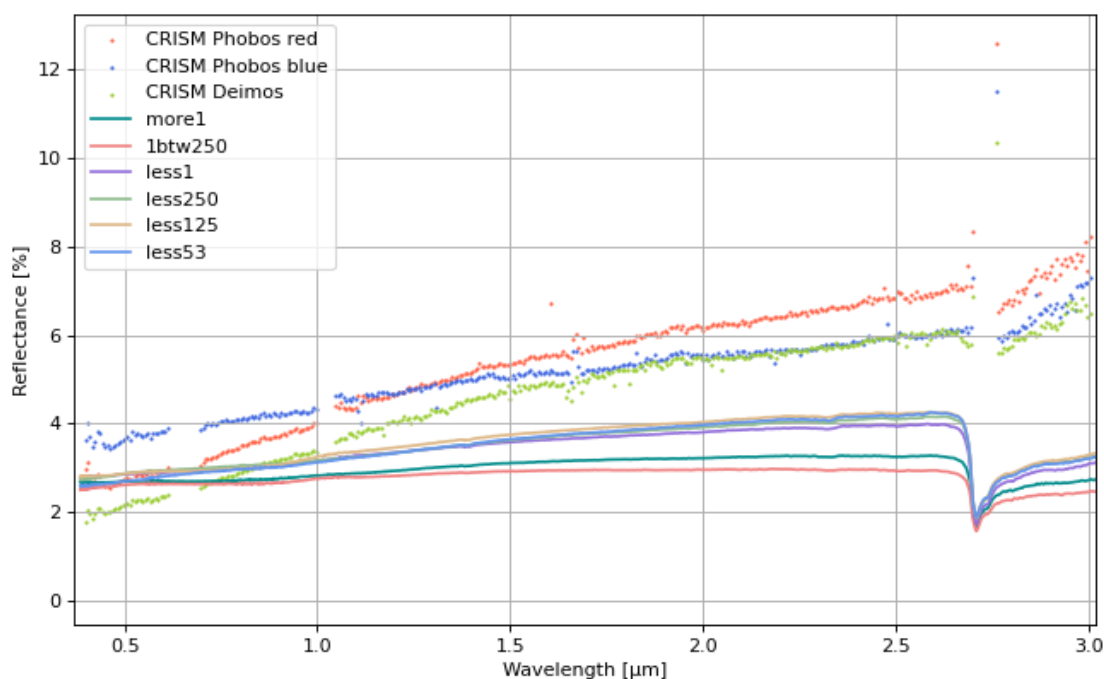

Figure 19 - UTPS-TB and CRISM spectra in range 0.38 to 3.0µm.

UTPS-TB OROCHI SPECTRA

The UTPS-TB have been studied in OROCHI instrument conditions. The Figure corresponds to their resulting spectra, without CRISM data as in Simulation of the results in OROCHI conditions part.
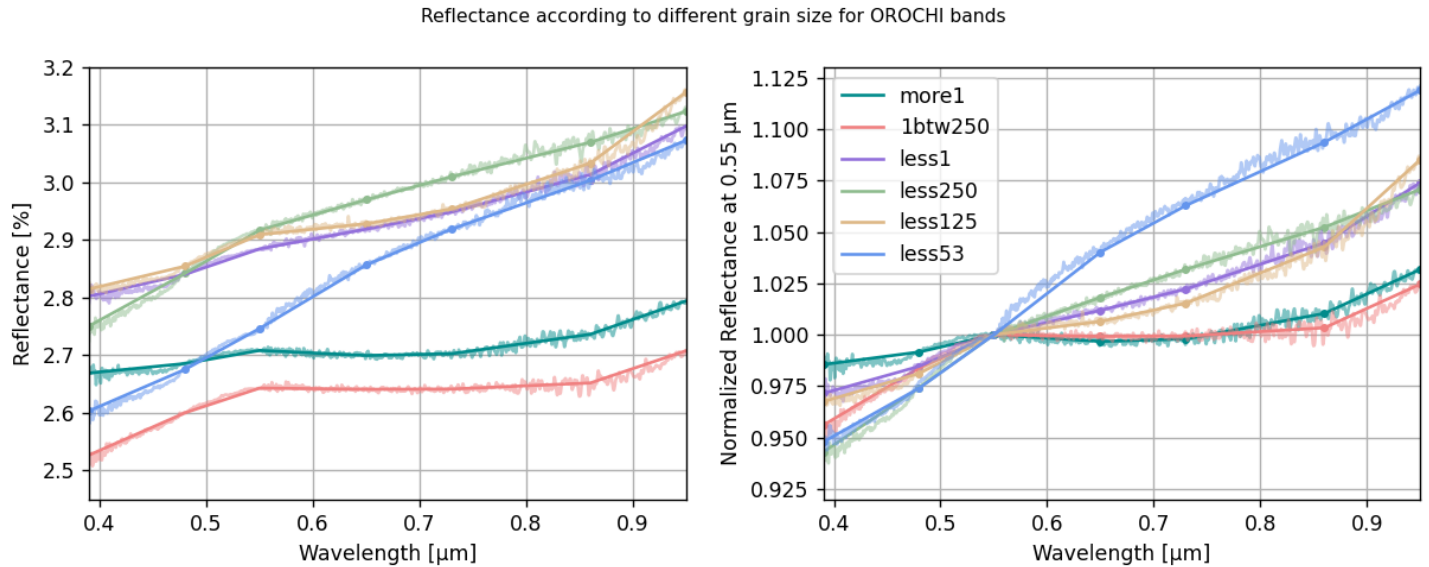

Figure 20 - OROCHI expected results according to its filter bands. (left) Reflectance spectrum (right) Normalized reflectance at 0.55µm. The letters represent the band given in Table 4. The blurry signals are the raw signals from UTPS-TB and the straight lines are the average values obtained in OROCHI conditions.

THERMAL EMISSION EFFECT ON REFLECTANCE SPECTRA

The effect of thermal inertia is described in Figure 21.
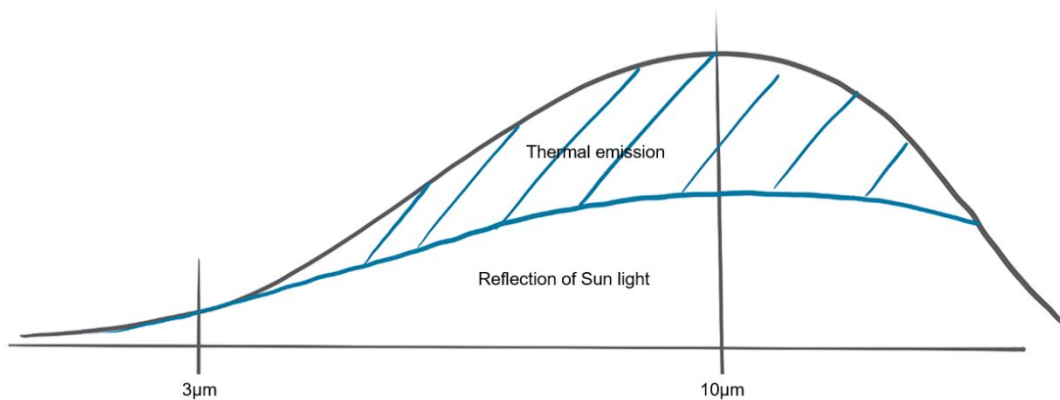

Figure 21 - Effect of thermal emission on reflectance spectra. The blue part corresponds to thermal emission effect, whereas the real reflectance is above that blue part. The 10µm range corresponds to the maximum value and 3µm is the location of MIRS study.

Effects of organics on reflectance intensity and features

The organics reduce are darkening spectra and have a masking effect on the features for smallest wavelengths. The spectra are coming from (Giuranna et al. 2011) paper.
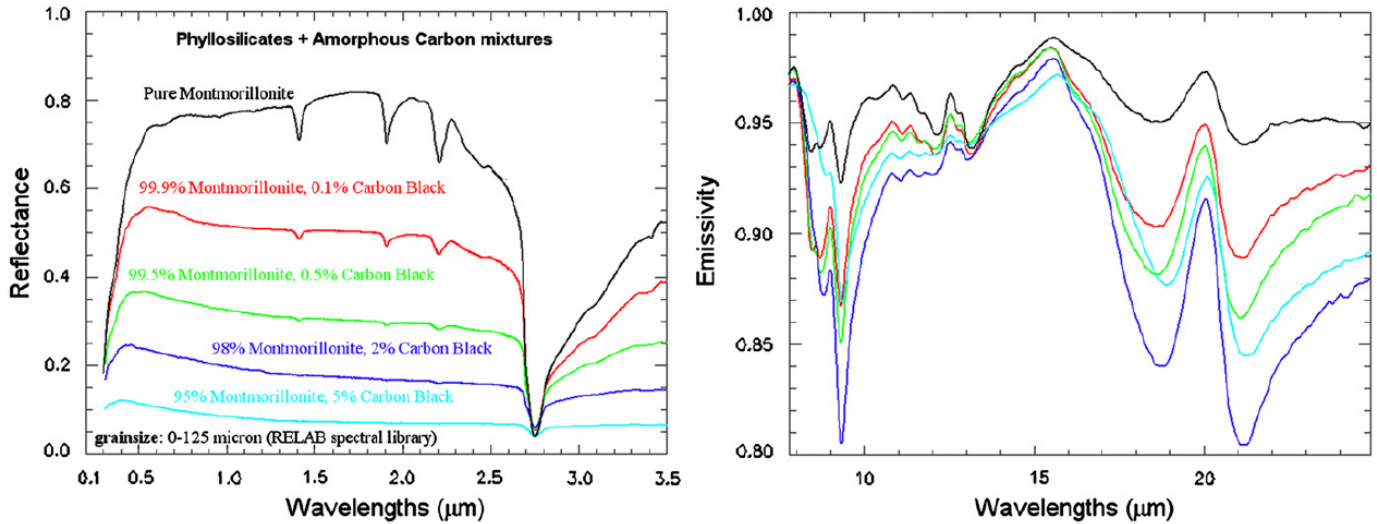

Fig. 15. Reflectance (a) and emissivity (b) spectra of montmorillonite (M) mixed with carbon black (CB). Black curve: pure montmorillonite. Red curve: 99.9% M, 0.1% CB. Green curve: 99.5% M, 0.5% CB. Blue curve: 98% M, 2% CB. Cyan curve: 95% M, 5% CB. Samples grain size: < 125 µm.

Figure 22 - Effect of organics on reflectance intensity and features.